Journal of
Micro/Nanolithography,
MEMS, and MOEMS

Nanolithography.SPIEDigitalLibrary.org

Influence of template fill in graphoepitaxy directed self-assembly

Jan Doise
Joost Bekaert
Boon Teik Chan
SungEun Hong
Guanyang Lin
Roel Gronheid

SPIE.

Jan Doise, Joost Bekaert, Boon Teik Chan, SungEun Hong, Guanyang Lin, Roel Gronheid, "Influence of template fill in graphoepitaxy directed self-assembly," *J. Micro/Nanolith. MEMS MOEMS* **15**(3), 031603 (2016), doi: 10.1117/1.JMM.15.3.031603.

Influence of template fill in graphoepitaxy directed self-assembly

Jan Doise,[a,b,*] Joost Bekaert,[b] Boon Teik Chan,[b] SungEun Hong,[c] Guanyang Lin,[c] and Roel Gronheid[b]
[a]KU Leuven, Department of Electrical Engineering (ESAT), Kasteelpark Arenberg 10, B-3001 Heverlee, Belgium
[b]IMEC, Kapeldreef 75, B-3001 Heverlee, Belgium
[c]EMD Performance Materials Corp., 70 Meister Avenue, Somerville, New Jersey 08876, United States

Abstract. Directed self-assembly (DSA) of block copolymers (BCP) is considered a promising patterning approach for the 7-nm node and beyond. Specifically, a graphoepitaxy process using a cylindrical phase BCP may offer an efficient solution for patterning randomly distributed contact holes with subresolution pitches, such as found in via and cut mask levels. In any graphoepitaxy process, the pattern density impacts the template fill (local BCP thickness inside the template) and may cause defects due to over- or underfilling of the template. In order to tackle this issue thoroughly, the parameters that determine template fill and the influence of template fill on the resulting pattern should be investigated. Using three process flow variations (with different template surface energy), template fill is experimentally characterized as a function of pattern density and film thickness. The impact of these parameters on template fill is highly dependent on the process flow, and thus prepattern surface energy. Template fill has a considerable effect on the pattern transfer of the DSA contact holes into the underlying layer. Higher fill levels give rise to smaller contact holes and worse critical dimension uniformity. These results are important for DSA-aware design and show that fill is a crucial parameter in graphoepitaxy DSA. [DOI: 10.1117/1.JMM.15.3.031603]

Keywords: directed self-assembly; graphoepitaxy; pattern density; film thickness; template fill.

Paper 16032SSP received Apr. 1, 2016; accepted for publication Jul. 15, 2016; published online Aug. 17, 2016.

1 Introduction

Directed self-assembly (DSA) of block copolymers (BCPs) has received a great deal of research attention as a potential patterning approach for future generation integrated circuit fabrication. One of the DSA schemes that is considered to have a high potential to be integrated into device manufacturing in the near future is the patterning of contact holes by using graphoepitaxy with a cylindrical phase BCP[1–3] (at IMEC referred to as templated DSA). In graphoepitaxy, lithography is used to create a topographical prepattern in which a BCP is deposited and allowed to phase separate. In case a cylindrical phase BCP is applied, this gives a straightforward approach to pattern randomly distributed contact holes. Insertion of DSA in this way offers the opportunity of reduction of cost and processing time compared to conventional multiple patterning techniques by reducing the number of needed masks.[2,4]

In order for implementation of graphoepitaxy DSA into device manufacturing to be successful, a number of challenges still need to be addressed. Among those are defectivity, pattern placement accuracy, and DSA-aware design. It has been previously reported that graphoepitaxy processes show a dependence on template pattern density.[5,6] Commonly, it has been observed that the pattern density impacts the template fill (local BCP thickness prior to wet development, see Fig. 1) and may cause defects such as missing and merging contact holes due to over- or underfilling of the template. A potential solution to this problem is to increase the uniformity of the pattern density in the design by including sub-DSA-resolution assist features[4,7,8] to regions with lower density. An alternative approach is DSA planarization.[9]

However, in order to thoroughly address this issue, it is crucial to get more insight into all parameters that determine template fill. In addition, the influence of template fill on the resulting morphology and the subsequent pattern transfer should be investigated. Until now, only limited studies (experimental or simulation[10]) are available on this matter. In previous work, we have roughly estimated template fill based on an empirical formula in order to construct process windows.[11,12] This works aims to do a more comprehensive experimental investigation of this topic using atomic force microscopy (AFM) to accurately measure the template fill. First, template fill is shown to depend on pattern density, film thickness, and prepattern surface energy. Afterward, findings are presented concerning the influence of template fill on the resulting DSA morphology and the transfer of the DSA pattern into the underlying layer.

2 Experimental

2.1 *Process and Materials*

Guiding templates were patterned on 300-mm wafers using an ASML NXT:1950i scanner linked to a Sokudo DUO coat and development system. A trilayer stack consisting of 100 nm of spin-on-carbon (SOC, HM710 from JSR Micro), 30 nm of spin-on-glass (SOG, ISX304 from JSR Micro), and 85 nm of ArF immersion negative tone development photoresist (AN02 from Fujifilm) were deposited on top of a Si_3N_4 substrate. For coating and development of

*Address all correspondence to: Jan Doise, E-mail: jan.doise@imec.be

1932-5150/2016/$25.00 © 2016 SPIE

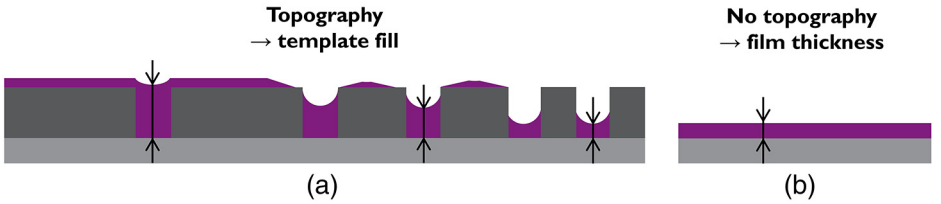

Fig. 1 (a) Schematic representation of template fill, the local BCP thickness inside a template and (b) film thickness, the film height on a topographically flat wafer under identical coating conditions.

the trilayer stack, vendor recommended settings were used for postapply bake, postexposure bake, and development. Exposures were done at 1.2 NA using annular illumination with $\sigma_o = 0.8$, $\sigma_i = 0.6$, and XY-polarization. The templates defined in resist were then transferred into the underlying SOG and SOC by a dry etch process carried out on a Tokyo Electron Tactras™ platform. Finally, unless otherwise noted, SOG was removed using 0.5% HF on a Tokyo Electron CELLESTA™ wafer clean system.

All DSA processing steps were done on a Tokyo Electron CLEAN TRACK ACT 12™ or CLEAN TRACK LITHIUS Pro Z™. Brush-A and brush-B were synthesized by EMD Performance Materials and were used as received. The brushes were spin-coated from solution and subsequently thermally annealed under a nitrogen atmosphere. Afterward, ungrafted polymer molecules were removed with an organic solvent (RER600 from Fujifilm) rinse. Subsequently, a cylindrical phase poly(styrene-block-methyl methacrylate) BCP (AZEMBLY™ PME-585, from EMD Performance Materials) with an unguided pitch of 37 nm was spin-coated from solution (at various spin speeds and viscosities) and subsequently thermally annealed under a nitrogen atmosphere. The poly(methyl methacrylate) (PMMA) cores were removed by deep ultraviolet exposure followed by an isopropyl alcohol rinse. Finally, pattern transfer of the DSA holes into the underlying Si_3N_4 was carried out on a Tokyo Electron Tactras™ platform.

2.2 *Metrology*

Images obtained using a Hitachi CG-5000 top-down critical dimension scanning electron microscope (CD-SEM) were analyzed using robust edge detection software from Hitachi to determine the CD of templates (after SOG strip) and DSA contact holes (after PMMA removal and after pattern transfer into Si_3N_4). Reported CD (or local CD uniformity) values are averages (or three sigma values) of at least 100 individual contacts, the number of images taken depending on the template pitch. Similarly, to determine open hole rate, at least 100 individual contacts were inspected. An NX-3DM (noncontact) AFM from Park Systems, equipped with a M-CNT150 tip from Nanotools, was used to obtain a 1-μm^2 scan of the topography after BCP anneal. The template fill was then calculated from the template height and the maximum depth for each template (for more information, see Appendix A). Film thickness was measured using a KLA-Tencor SCD-100 ellipsometer.

3 Results and Discussion

3.1 *Process flow for Templated Directed Self-Assembly*

The process flow for templated DSA at IMEC is schematically shown in Fig. 2. This work uses three variations of this process flow that have been described previously in detail.[11] In short, in the first variation (flow #1), the BCP is coated directly after the dry etch process that defines the templates—without any prior surface energy modification. The other variants have the SOG strip and use different polymer brushes. In flow #2, a neutral brush, brush-A, is used. This brush grafts at a higher rate to the Si_3N_4 bottom (compared to the SOC sidewalls), resulting in a nonpreferential bottom surface while maintaining PMMA-wetting sidewalls. In contrast, the brush used in flow #3 (brush-B) has a higher styrene content and grafts at a higher rate to the SOC, altering the SOC sidewalls to have an affinity for PS while at the same time modifying the bottom surface to be nonpreferential.

The resulting different interfacial energies of the three flows impact the three-dimensional (3-D) structure of the BCP inside the template as well as the ideal template

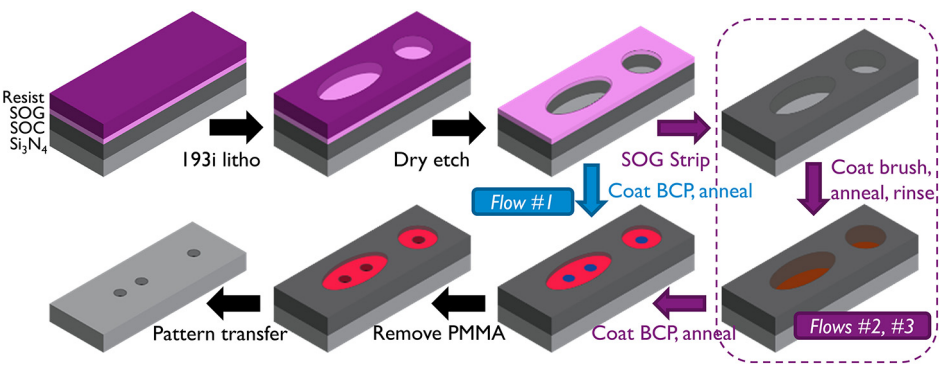

Fig. 2 Schematic overview of the process flow for templated DSA.

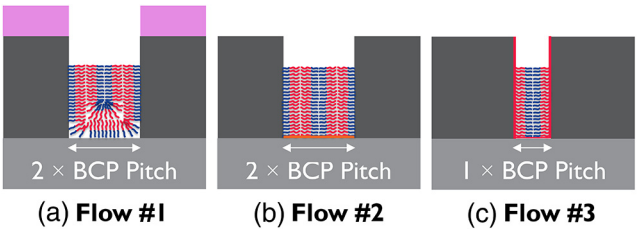

Fig. 3 Schematic representation of arrangement of BCP chains in a template for (a) flow #1, (b) flow #2, and (c) flow #3.

dimensions for commensurability with the BCP pitch. This is schematically shown in Fig. 3.

3.2 *Analysis of Phenomena Influencing Template Fill*

In order to investigate the influence of different parameters on template fill, wafers were fabricated containing templates with the same dimensions but at different pitches (and thus different pattern densities). The template dimensions for each flow were chosen to be in the center of their corresponding process window for singlets (single hole shrink patterns), which was determined in previous work.[11] Template CDs of 73, 68, and 50 nm in SOC were used for flow #1, flow #2, and flow #3, respectively. More details on template CD and local CD uniformity (LCDU) can be found in Appendix B. Additionally, duplicate wafers were coated with different BCP film thicknesses (i.e., the thickness measured using ellipsometry on a topographically flat wafer under identical coating conditions, see Fig. 1). Figure 4 shows the template fill as measured by AFM as a function of pattern density and film thickness for each flow. As expected from earlier reports, for all three flows, higher fill values are measured at lower pattern densities and higher film thicknesses. However, the impact of these parameters is considerably different for each flow. For flow #1, both the film thickness and the pattern density can cause large changes in the resulting template fill. For flow #2, the effect of pattern density is again large, whereas the influence of film thickness is more limited, although still significant. Finally, for flow #3, both parameters have only a limited degree of influence on the resulting template fill. Our hypothesis is that the difference in surface energy of the top surface of the prepattern is the main cause for this difference in fill behavior. This surface energy will play a role in the mass transfer of BCP molecules across the surface during the BCP anneal. Flow #1 has the most hydrophilic top surface (as a result of the dry etch), whereas flow #3 has the most hydrophobic top surface (due to brush-B). Other factors that could play a role are the increased template height for flow #1 due to the remaining SOG and the comparatively smaller template size for flow #3.

In addition to pattern density and film thickness, local BCP assembly phenomena can influence the template fill. We will illustrate this with two examples. In the first example (shown in Fig. 5), we observe an increasing number of closed holes at high fill levels (starting from a fill of ~90 nm) for flow #1. As can be seen in the SEM image, the BCP assembles into a PMMA ring at the top of the template. After PMMA removal, this morphology results in a closed hole. In the AFM scan, we can see a significant increase in fill for these templates. This suggests that the BCP reflows

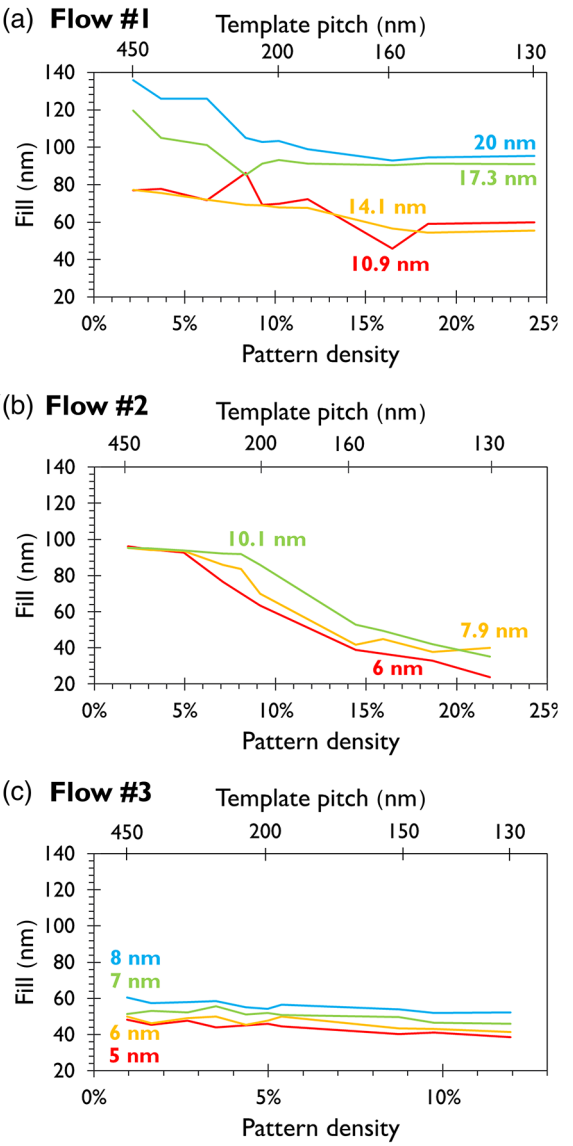

Fig. 4 Template fill as measured by AFM as a function of pattern density and film thickness for (a) flow #1, (b) flow #2, and (c) flow #3.

during the annealing step to assemble into this morphology. In the second example (shown in Fig. 6), we can see a related effect occurring for flow #2. Here, the BCP assembles to form additional adjacent PMMA cylinders, in a hexagonal arrangement, on the top surface. Similar to the first example, an increase in fill level (although less substantial compared to flow #1) is measured at these locations. In conclusion, the rearrangement of BCP chains to the lowest energy configuration can have an influence on the template fill. This phenomenon does not cause any defects after PMMA removal for flow #2, but it does result in a higher variation in fill level, which in turn might worsen the variation in CD after pattern transfer (as will be discussed later).

3.3 *Influence of Fill on Pattern Quality*

Figure 7 lists the open hole rate for each flow as a function of template pitch and film thickness as determined by top-down inspection after PMMA removal and after pattern transfer. It can be seen that only flow #3 offers 100% open hole rates for

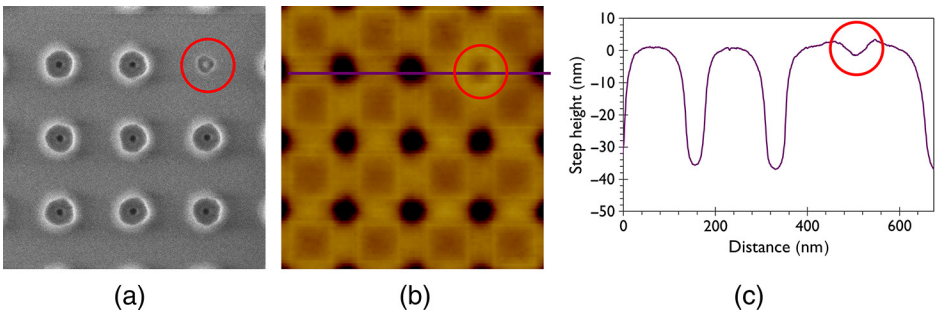

Fig. 5 (a) Top-down CD-SEM image of singlets after PMMA removal at high fill level for flow #1, (b) the corresponding AFM image after BCP anneal, and (c) AFM step height curve. The BCP assembles into a PMMA ring at the top of the template (red circle). With AFM, a significantly increased fill level is observed.

all pitches with one film thickness after pattern transfer. For flow #1, at low template fill, no holes are observed after PMMA removal as well as after pattern transfer. It is assumed that the preferential wetting at the bottom of the template causes this defective assembly, as this is not observed for the other flows at even lower fill levels (see Fig. 8). At higher fill levels, as previously shown in Fig. 5, we observe an increase in closed holes as the BCP assembles into unwanted morphologies. Flow #2 offers good open hole rates after PMMA removal regardless of fill level, but missing holes are observed after pattern transfer at higher fill levels. This is likely caused by aspect ratio dependent etching. As the fill levels for flow #2 range from around 23 to 96 nm for the different template pitches (at a film thickness of 6 nm), this means the aspect ratio of the holes range from ∼1 : 1.5 to 1:6. Higher aspect ratio holes are expected to etch more slowly as etchants are more difficult to pass through and etch byproducts are harder to diffuse out. In addition, polymerizing species may block the higher aspect ratio holes more easily. In contrast, for flow #3, the fill levels range from 38 to 48 nm (at a film thickness of 5 nm) which corresponds to a much smaller variation in aspect ratio of the holes, from ∼1 : 2 to 1:3.

Figure 9 shows contact hole CD and LCDU (3σ values) as a function of template fill for each flow, after PMMA removal as well as after pattern transfer in the silicon nitride. We can observe that, for each flow, the template fill does not have a significant impact on the CD after PMMA removal, with rather constant values around 15, 17, and 18 nm measured for flow #1, flow #2, and flow #3, respectively. This is in contrast to the CDs measured after pattern transfer. For flows #2 and #3, a close to linear relationship is found between template fill and the resulting CD after pattern transfer, with smaller CDs observed for increasing template fill. For flow #1, the CD after pattern transfer first increases to a maximum at a fill around ∼85 nm at which it starts decreasing again. Our hypothesis is that this is caused by changes in the 3-D morphology associated with this flow.

Concerning the influence of fill on LCDU, similar observations can be made. No substantial impact is seen after PMMA removal, with LCDU values slowly decreasing from 4 to 3 nm with increasing fill. It is difficult to determine if the root cause of this trend is related to the BCP assembly or metrology, as higher fill levels generally give better contrast in the SEM images. After transfer into the silicon nitride, much more substantial changes can be noticed. In general, higher fill levels result in worse LCDU. This can be explained by higher aspect ratios giving way to more variations in the etch process, as well as a larger variation in fill level (see example in Fig. 6) causing variations in CD after pattern transfer. The only exception to this is for flow #1, where the LCDU shows a minimum at a fill around ∼85 nm that corresponds to the maximum in CD.

4 Conclusions

In this work, template fill is shown to depend on numerous parameters and phenomena, such as pattern density, film thickness, template surface energy, and local assembly effects. Film thickness and pattern density are the main parameters to control, but their impact can vary significantly for different flows (with different surface energy). From the flows investigated in this work, flow #3 (with PS-wetting

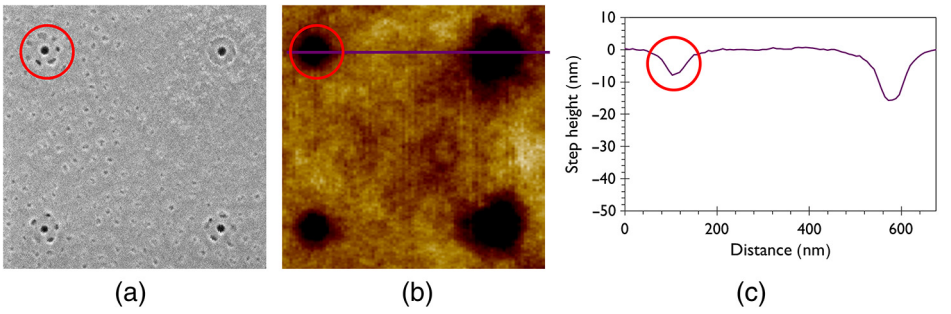

Fig. 6 (a) Top-down CD-SEM image of singlets after PMMA removal at high fill level for flow #2, (b) the corresponding AFM image after BCP anneal, and (c) AFM step height curve. At high fill levels, the BCP may assemble to form adjacent PMMA cylinders in hexagonal arrangement (red circle). With AFM, an increased fill level is observed.

(a) **Flow #1**

Template pitch (nm) →

After PMMA removal

Film thickness (nm)	130	150	160	187.5	200	212.5	225	255	340	450
10.9	0.0%	0.0%	0.0%	100.0%	100.0%	100.0%	92.3%	100.0%	100.0%	100.0%
14.1	0.0%	100.0%	99.5%	100.0%	99.5%	100.0%	100.0%	98.6%	100.0%	100.0%
17.3	0.0%	100.0%	100.0%	100.0%	100.0%	100.0%	99.5%	96.6%	91.4%	71.9%
20	100.0%	99.5%	100.0%	97.6%	87.0%	90.3%	77.8%	51.2%	0.0%	0.0%

After pattern transfer

Film thickness (nm)	130	150	160	187.5	200	212.5	225	255	340	450
10.9	0.0%	0.0%	0.0%	98.6%	99.5%	100.0%	96.1%	100.0%	98.4%	99.2%
14.1	0.0%	99.0%	100.0%	100.0%	100.0%	100.0%	100.0%	100.0%	100.0%	99.2%
17.3	76.0%	99.5%	100.0%	100.0%	99.5%	100.0%	100.0%	99.0%	84.4%	70.3%
20	100.0%	100.0%	100.0%	92.3%	90.3%	86.5%	79.2%	58.9%	0.0%	0.0%

(b) **Flow #2**

Template pitch (nm) →

After PMMA removal

Film thickness (nm)	130	140	150	160	200	212.5	225	270	340	450
6	100.0%	100.0%	100.0%	100.0%	100.0%	100.0%	100.0%	100.0%	100.0%	100.0%
7.9	100.0%	100.0%	100.0%	100.0%	100.0%	100.0%	100.0%	100.0%	100.0%	100.0%
10.1	100.0%	100.0%	100.0%	99.0%	100.0%	100.0%	100.0%	100.0%	100.0%	100.0%

After pattern transfer

Film thickness (nm)	130	140	150	160	200	212.5	225	270	340	450
6	100.0%	100.0%	99.5%	100.0%	100.0%	99.0%	100.0%	98.4%	93.8%	97.7%
7.9	100.0%	100.0%	100.0%	100.0%	98.6%	99.0%	98.6%	90.6%	93.0%	83.6%
10.1	100.0%	100.0%	100.0%	100.0%	100.0%	95.2%	90.3%	65.6%	76.6%	50.0%

(c) **Flow #3**

Template pitch (nm) →

After PMMA removal

Film thickness (nm)	130	140	150	187.5	200	212.5	240	270	340	450
5	100.0%	100.0%	100.0%	100.0%	98.1%	100.0%	100.0%	99.2%	100.0%	100.0%
6	100.0%	100.0%	100.0%	100.0%	100.0%	100.0%	100.0%	100.0%	100.0%	100.0%
7	100.0%	100.0%	100.0%	100.0%	100.0%	100.0%	100.0%	100.0%	100.0%	100.0%
8	100.0%	100.0%	100.0%	99.0%	100.0%	99.0%	100.0%	100.0%	100.0%	100.0%

After pattern transfer

Film thickness (nm)	130	140	150	187.5	200	212.5	240	270	340	450
5	100.0%	100.0%	100.0%	100.0%	100.0%	100.0%	100.0%	100.0%	100.0%	100.0%
6	100.0%	100.0%	100.0%	100.0%	100.0%	100.0%	100.0%	100.0%	100.0%	100.0%
7	100.0%	100.0%	100.0%	100.0%	100.0%	100.0%	100.0%	100.0%	100.0%	100.0%
8	100.0%	100.0%	100.0%	100.0%	100.0%	99.5%	99.5%	99.2%	98.4%	100.0%

Fig. 7 Open hole rate after PMMA removal and after pattern transfer as a function of pitch and film thickness for (a) flow #1, (b) flow #2, and (c) flow #3.

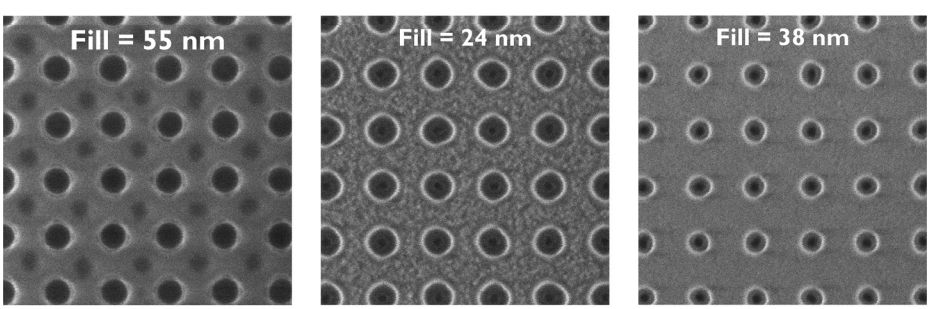

Fig. 8 Top-down CD-SEM images of singlets after PMMA removal at low fill levels. (a) For flow #1, closed holes are observed. (b) Flows #2 and (c) #3 show open holes at even lower template fill.

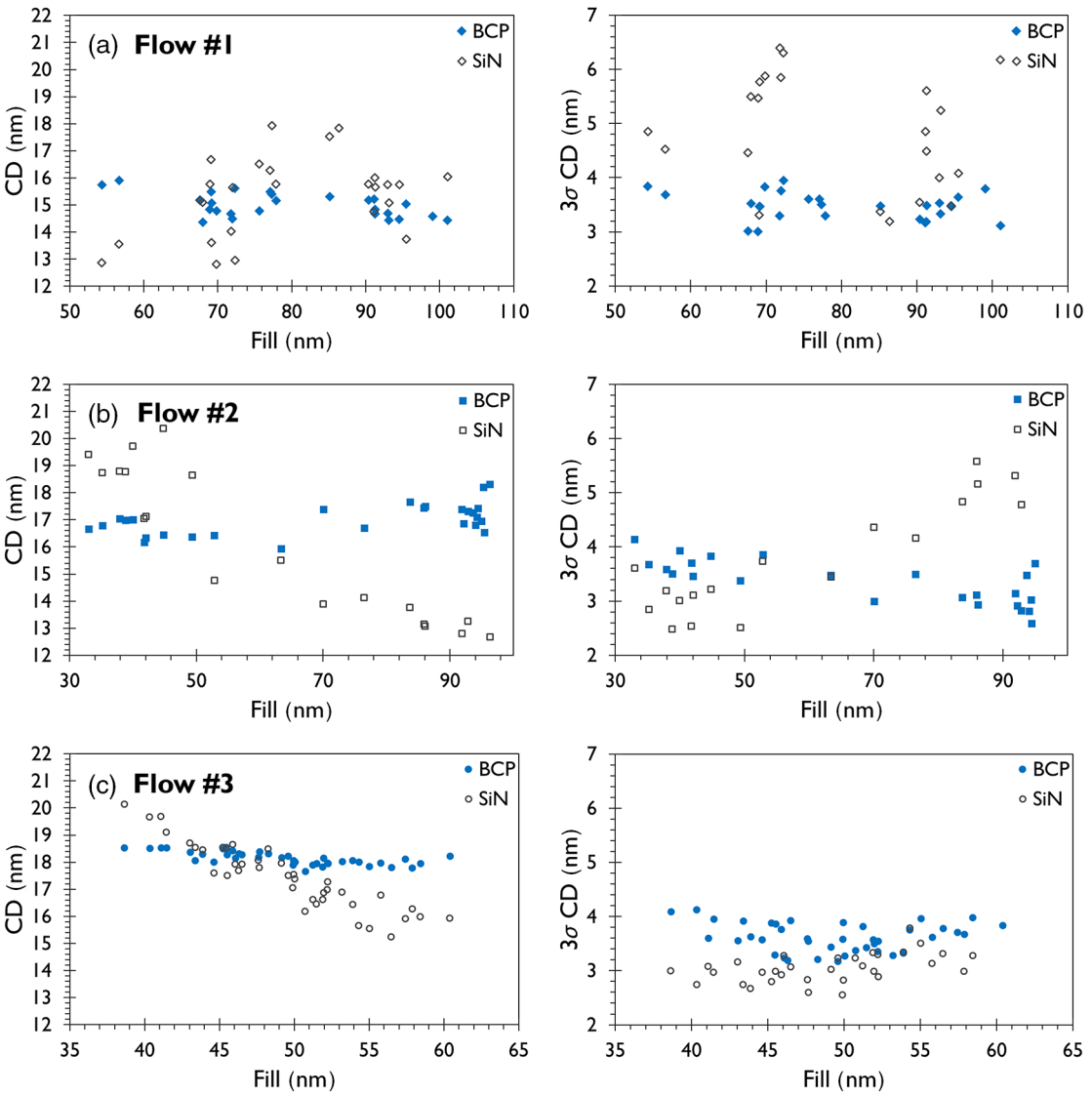

Fig. 9 Contact hole CD and LCDU (3σ values) for (a) flow #1, (b) flow #2, and (c) flow #3 after PMMA removal (BCP) as well as after pattern transfer (SiN) as a function of template fill.

sidewalls and top surface) is the least sensitive to changes in pattern density. Next, the influence of template fill on the resulting pattern quality was investigated after BCP assembly and after pattern transfer. In the case of flow #1 (template bottom preferential to PMMA), the morphology is very sensitive to the fill level, with defects found at too low as well as at too high values of template fill. Regardless of the process flow used, template fill has a

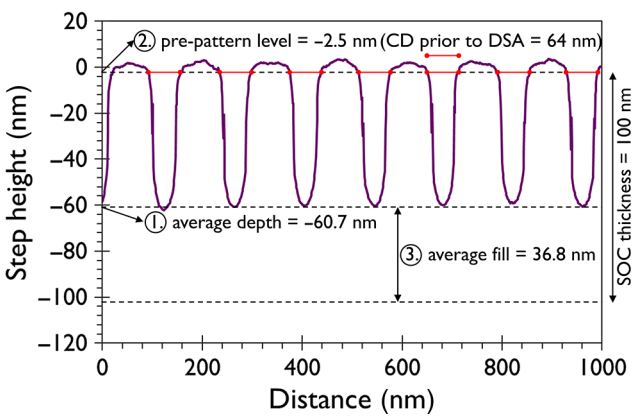

Fig. 10 Procedure of calculating the template fill from the AFM measurement for templates prepared with flow #2.

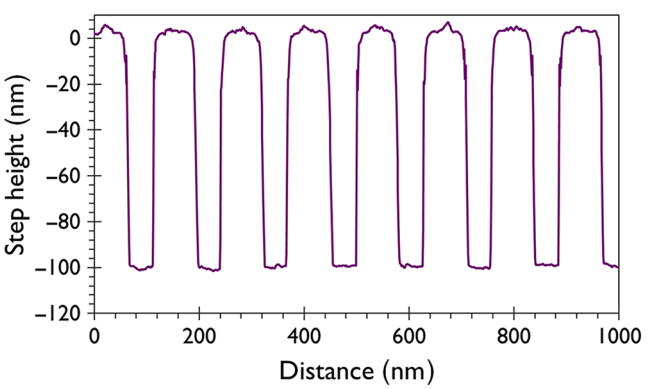

Fig. 11 The AFM step height curve for templates with a CD of 50 nm prior to DSA processing indicates that the AFM tip successfully reaches the bottom of the pattern.

(a) **Flow #1** Template pitch (nm) →

	130	150	160	187.5	200	212.5	225	255	340	450
CD (nm)	72.3	72.7	73.2	72.7	72.0	73.1	73.4	71.9	73.8	74.6
LCDU (nm)	5.2	4.0	3.9	4.2	4.3	3.8	4.2	3.9	5.2	4.4

(b) **Flow #2** Template pitch (nm) →

	130	140	150	160	200	212.5	225	270	340	450
CD (nm)	68.5	68.3	67.6	68.6	68.3	68.3	67.6	67.7	67.5	69.1
LCDU (nm)	4.1	3.7	3.5	3.5	3.6	3.3	3.7	3.2	3.4	3.3

(c) **Flow #3** Template pitch (nm) →

	130	140	150	187.5	200	212.5	240	270	340	450
CD (nm)	50.7	49.3	50.1	49.0	50.4	50.1	50.7	49.9	49.2	49.4
LCDU (nm)	4.5	4.5	4.2	4.2	3.7	3.4	3.9	3.6	3.8	3.7

Fig. 12 Template CD and LCDU values measured with CD-SEM for (a) flow #1, (b) flow #2 and (c) flow #3.

significant impact on the CD after pattern transfer and higher fill levels give rise to worse LCDU performance. This learning is important for DSA-aware design and show that template fill is an important parameter in graphoepitaxy DSA.

Appendix A: Atomic Force Microscopy Metrology Details

To correctly determine the fill level from the AFM measurement, the following procedure was used (shown in Fig. 10):

1. The maximum depth of each template was determined and the average "maximum depth" was calculated.
2. The level of the SOC (for flows #2 and #3) or SOG (for flow #1) prepattern in the AFM measurement was determined. Since a part of the BCP material ends up on top of the prepattern after DSA, the highest level in the AFM measurement does not necessarily correspond to the height of the prepattern prior to DSA. In order to extract this value as correctly as possible, the CD of the template prior to DSA (measured with CD-SEM) was used to estimate the original height of the prepattern. In the example in Fig. 10, this CD is equal to 64 nm (for flow #2, the 68 nm SOC template shrinks 4 nm after brush application prior to DSA).
3. The average fill was calculated from these two numbers and the template height (130 nm for flow #1 and 100 nm for flows #2 and #3).

In order to verify that the AFM tip successfully reaches the bottom of the pattern, a wafer with empty templates (prior to any DSA processing) with a CD of 50 nm was measured. The results (shown in Fig. 11) indicate that the AFM tip provides a reliable readout of the template fill.

Appendix B: Template Critical Dimension and Local Critical Dimension Uniformity Details

A point of attention in this study was the impact of template CD and LCDU on the fill. Since a change in template CD corresponds to a change volume, this is another factor that influences the fill (or fill variation). Our goal was to keep this parameter as constant as possible, and compare the different flows at a fixed CD, chosen to be optimal for the respective flow. Therefore, mask CD, pitch, and illumination conditions were carefully chosen in order to have similar template CD and LCDU for the different pitches as well as similar LCDU for the different flows. These data are shown in Fig. 12.

Acknowledgments

Jan Doise gratefully acknowledges the support of a PhD stipend from the Agency for Innovation by Science and Technology (IWT). The authors wish to thank Tae-Gon Kim and Henry Ryu for carrying out the AFM measurements.

References

1. H. Kato et al., "Sub-30 nm via interconnects fabricated using directed self-assembly," *Microelectron. Eng.* **110**, 152–155 (2013).
2. Y. Ma et al., "Challenges and opportunities in applying grapho-epitaxy DSA lithography to metal cut and contact/via applications," *Proc. SPIE* **9231**, 92310T (2014).
3. J. Y. Cheng et al., "Simple and versatile methods to integrate directed self-assembly with optical lithography using a polarity-switched photoresist," *ACS Nano* **4**(8), 4815–4823 (2010).
4. J. Bekaert et al., "N7 logic via patterning using templated DSA: implementation aspects," *Proc. SPIE* **9658**, 965804 (2015).
5. R. Gronheid et al., "Process optimization of templated DSA flows," *Proc. SPIE* **9051**, 90510I (2014).
6. P. Pimenta Barros et al., "Etch challenges for DSA implementation in CMOS via patterning," *Proc. SPIE* **9054**, 90540G (2014).
7. H. Yi et al., "Experimental study of sub-DSA resolution assist features (SDRAF)," *Proc. SPIE* **9423**, 94231F (2015).
8. A. Latypov and T. H. Coskun, "DSA-aware assist features," *Proc. SPIE* **9423**, 94231G (2015).
9. P. Pimenta Barros et al., "DSA planarization approach to solve pattern density issue," *Proc. SPIE* **9428**, 94280D (2015).
10. H. Yi, A. Latypov, and H.-S. P. Wong, "Computational simulation of block copolymer directed self-assembly in small topographical guiding templates," *Proc. SPIE* **8680**, 86801L (2013).
11. J. Doise et al., "Implementation of surface energy modification in graphoepitaxy directed self-assembly for hole multiplication," *J. Vac. Sci. Technol. B* **33**(6), 06F301 (2015).
12. R. Gronheid et al., "Implementation of templated DSA for via layer patterning at the 7 nm node," *Proc. SPIE* **9423**, 942305 (2015).

Jan Doise is a PhD student working on directed self-assembly of block copolymers at KU Leuven and IMEC. He obtained his MS degree in nanoscience and nanotechnology from KU Leuven in 2013.

Biographies for the other authors are not available.